ASME 2012 5th Annual Dynamic Systems and Control Conference joint with the JSME 2012 11th Motion and Vibration Conference
DSCC2012-MOVIC2012
October 17-19, 2012, Fort Lauderdale, Florida, USA

DSCC2012-MOVIC2012-8846

ROBOCATH: A PATIENT-MOUNTED PARALLEL ROBOT TO POSITION AND ORIENT SURGICAL CATHETERS

Amirhossein Salimi[*]
Amin Ramezanifar
Dept. of Mechanical Engineering
University of Houston
Houston, TX 77204
Email: asalimi@uh.edu

Javad Mohammadpour[†]
Dept. of Naval Architecture & Marine Engineering
University of Michigan
Ann Arbor, MI 48109
Email: javadm@umich.edu

K. Grigoriadis
Dept. of Mechanical Engineering
University of Houston
Houston, TX 77204

N. V. Tsekos
Dept. of Computer Science
University of Houston
Houston, TX 77204

ABSTRACT

Hosting the cardiac catheters and the necessity for their precise and collision-free navigation in transapical beating-heart interventions require the development of dexterous and reliable robotic platforms. These mechanisms should not only be capable of tracking the desired trajectories with high level of accuracy but also have to have the potential to cope with strict medical constraints such as environment compatibility, patient safety and compactness. In this paper, we propose a robotic platform that takes into account the above mentioned requirements. Benefiting from a state-of-the-art parallel structure, this four degree-of-freedom MRI-compatible patient-mounted and cable-driven manipulator (that we name ROBOCATH) seeks to steer cardiac catheters under beating heart condition, while suitably addressing the deficiencies that currently used manipulators vastly suffer from. In addition to the detailed description of the robot design and its specifications, kinematic model along with some experimental results on the prototype are provided.

[*]Address all correspondence to this author.
[†]The author was with UH at the time of completing this work.

1 Introduction

Since the installation of the first digitally operated and programmable industrial robot in 1961 [1], it took nearly two decades for engineers and scientists to bring robots into the operating rooms [2]. While in mid 80's and early 90's, surgical manipulators were simply industrial robots slightly tailored to fit medical requirements, the fast evolution from the first generation of surgical robots to recent mechanisms introduced new manipulators as extremely dexterous and highly customized robotic arms. In the more recent systems, factors such as manipulability, environment compatibility, compactness, light weight, dexterity and versatility are precisely considered. These considerations have resulted in noticeably improved completion of medical interventions using robotic manipulators compared to manual procedures. The mechanism studied in this paper could serve as a platform, in which most of the factors described above are taken into account.

Being coupled with variety of different medical imaging modalities, surgical robotic platforms become even more effective and reliable in operating rooms. Unique modality features such as true 3D imaging, no ionizing radiation, and on-the-fly control of imaging parameters make magnetic resonance imaging (MRI) a competitive option among other modalities [3]. Over

the past two decades, several research groups have made attempts to design and test robotic systems for MRI-guided procedures, focusing on a wide range of anatomic organs such as brain, breast, prostate and heart. The interested reader is referred to [4] and many references therein. One of the latest surgical procedures that has recently attracted the attention of many research groups is the transapical beating-heart intervention. This approach significantly reduces the side effects in cardiopulmonary bypass procedures and results in faster patient recovery [5]. In 2008, development of a robotic system for transapical aortic valve implantation under MRI guidance in beating heart was reported in [6]. Later, the authors integrated their system with a novel pneumatically actuated valve delivery module and evaluated its performance through ex-vivo experiments in [7]. In another study, a cyber physical system aimed for robot assisted MR-guided aortic valve replacement was proposed in [3, 8]. Focusing on beating-heart intracardiac procedures, this study demonstrated the feasibility of using MRI for guiding robotic manipulators in sophisticated heart surgeries.

The objective of the present study is to develop an MRI-compatible robotic platform that can assist with cardiac interventions under beating heart condition. Considering the challenges that similar systems have encountered so far, ROBOCATH is aimed to improve the quality of afore-mentioned robotic procedures. To make the actuation system MRI-compatible, several solutions have been proposed in the literature. Manual actuation [9], use of hydraulic cylinders [10] and utilizing pneumatic systems as the source of actuation [11] are some of the alternatives for magnetic motors for this purpose. Lack of precise navigation, fluid leakage in cylinders and limited stiffness of motors as the consequence of air compressibility are the major drawbacks of implementing these methods respectively [4]. Most of the recent MRI-compatible actuation systems utilize the piezoelectric motors in which motion is produced through the vibration of piezoelectric ceramics. Although these motors are magnet-free, image artifacts are observed due to the high frequency electric currents [12]. To avoid the afore-mentioned drawbacks, in this study, we use the conventional electric motors and place them far from the sensitive areas to make ROBOCATH fully MRI-compatible. In order to transfer the generated torque to the robot's joints, a cable transmission system is developed. The configuration of the designed system allows for each link to be actuated in both directions only by reversing the rotation in the corresponding motors.

One of the most interesting and yet challenging issues that is frequently encountered in free beating heart interventions is the chest motion due to the breathing. Obviously, in cases where the robot is mounted on the patient couch or the scanner structure, this relative motion has to be canceled out using the control algorithm. An alternative is to develop a platform that can passively compensate for it. The concept of developing patient-mounted robots has been examined before in [13]. In a recent study, five examples of body-supported surgical robots were surveyed [14]. These robots were employed for surgical procedures such as hip and knee replacement, spinal needle insertion, ultrasound exams and endoscope manipulation. Another case which is close to our application is a patient-mounted robotic platform for CT-guided procedures, in which the designed 5-DOF parallel structure is claimed to be capable of meeting the requirements of most interventional radiology procedures [15]. To the best of our knowledge, no patient-mounted robotic platform for MRI-guided interventions has been introduced so far. Mounting the platform on the patient not only helps the system cope with relative chest motion with respect to the fixed frames but also enables us to achieve extreme compactness in our design. This compactness later results in improved accuracy and the safety, as well as the reduced cost. As a summary, we list in Table 1 the specifications that should be taken into account in the design of ROBOCATH along with the methods that we offer to meet these requirements.

Table 1. System specifications and solution methods

Requirement	Solution method
Accuracy	Parallel architecture
MRI-compatibility	Cable-driven actuation system
Motion compensation	Patient-mounted platform

In this paper, we first describe the design and manufacturing process, as well as the benefits that the developed system offers compared to the existing surgical robotic platforms. Integration of the designed parallel robot with additional platform components including imaging and controls (using dSPACE) will be further described. Finally, an experimental test bed is employed to show some of the preliminary results achieved on the prototyped system as proof-of-concept for the proposed ROBOCATH system.

2 Design of the Mechanism

ROBOCATH is aimed to handle in-plane positioning and orientation of the catheter's tip. This particular mission necessitates the development of a 5-DOF manipulator; however, since the end effector is axi-symmetric, one degree of freedom could be omitted leading to a 4-DOF configuration. Table 2 lists the specifications for the kinematic requirements of the catheter. These specifications are dictated mainly by the intracardiac interventions.

In this paper, a highly customized parallel structure is proposed for the design of ROBOCATH. The proposed design is inspired by some earlier works such as the mechanisms introduced in [16, 17]. In addition to the advantages that conventional parallel robots offer, our novel design helps to further customize the platform to perfectly match the kinematic requirements mentioned earlier. Figure 1 illustrates the kinematics of the designed

Table 2. Catheter's kinematic requirements

Degree of freedom	Motion
Longitudinal motion	$\pm$ 5cm
Transversal motion	$\pm$ 5cm
Sagittal plane angle	25°-35°
Frontal plane angle	$\pm$ 15°

robot. In order to ensure the proper operation of the system, a combination of 9 prismatic and revolute degrees of freedom in the mechanism are defined. The degrees of freedom that are closer to the base are driven by the actuators (DOFs 1-4), while rest are actuated passively (DOFs 5-9). This arrangement facilitates the remote actuation of the manipulator. Finally, the Roman numbers represent the provided degrees of freedom for the catheter.

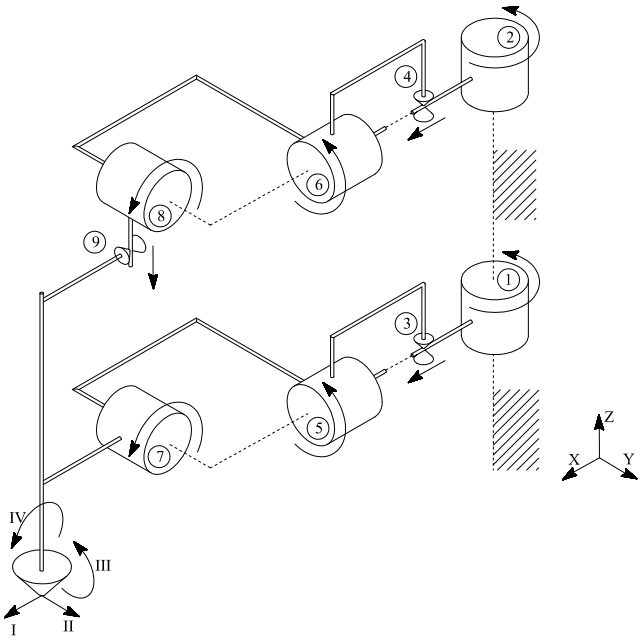

Figure 1. Kinematic of the structure

The detailed mechanical design of ROBOCATH is depicted in Figure 2. Two identical cylindrical mechanisms interconnected vertically, form the basic structure of the robot. Each subsystem consists of a fixed outer ring and an inner rotating ring. The outer cylinder is attached to the casing and hence forms the platform base. A radial bearing at the bottom section of each level makes it possible for the inner rings to have rotational motion with respect to the base. The remaining two degrees of freedom are generated by the linear motion of the two carriers sliding over the guide bars. The described rotational motions along with these two prismatic displacements form the desired four active degrees of freedom that was expected for the mechanism. These four active joints marked 1 to 4 in Figure 1, will later be actuated by motors through a cable transmission system. Each carrier has a universal joint at its center that acts like a liaison between the platform and the catheter. These passively actuated universal joints can eventually place the catheter in any desired orientations. While the distance between catheter's tip to the lower universal joint is kept constant, the distal end of the catheter is left to move freely with respect to the upper joint.

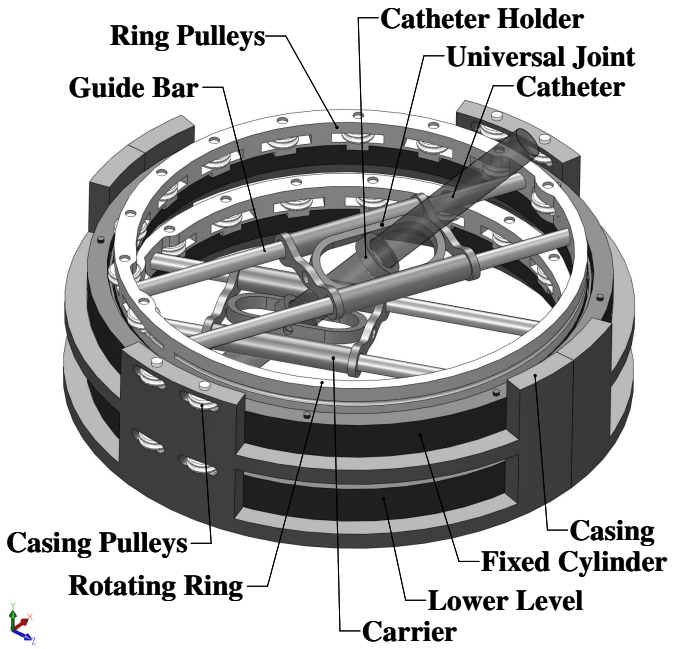

Figure 2. System architecture

3 Kinematics of the Designed Platform

In this section, we derive the forward and inverse kinematics corresponding to the proposed design of the mechanism described in the previous section.

3.1 Forward kinematics

To derive the equations corresponding to the forward kinematics of the mechanism, four different frames depicted in Figure 3 are defined as: (1) base frame $\{B\}$, which is fixed in the universal coordinate system and its Z-axis is in vertical direction, (2) lower frame $\{L\}$, which is attached to the center point of the lower cylinder with its Z-axis being along the vertical direction and the X-axis coinciding with the lower level linear direction, (3) upper frame $\{U\}$, which is the same as the lower frame except that it is placed at the center point of upper cylinder with its X-axis being along the upper sliding bar's center line and finally (4) end effector base $\{E\}$, which is attached to the catheter's center of mass with its Z-axis being along the catheter long axis. For each coordinate system, e.g. $\{B\}$, we call the unit vectors indicating principle directions as $\hat{\mathbf{X}}_B$, $\hat{\mathbf{Y}}_B$ and $\hat{\mathbf{Z}}_B$. In addition to the afore-mentioned frames, there are two other frames $\{UE\}$ and

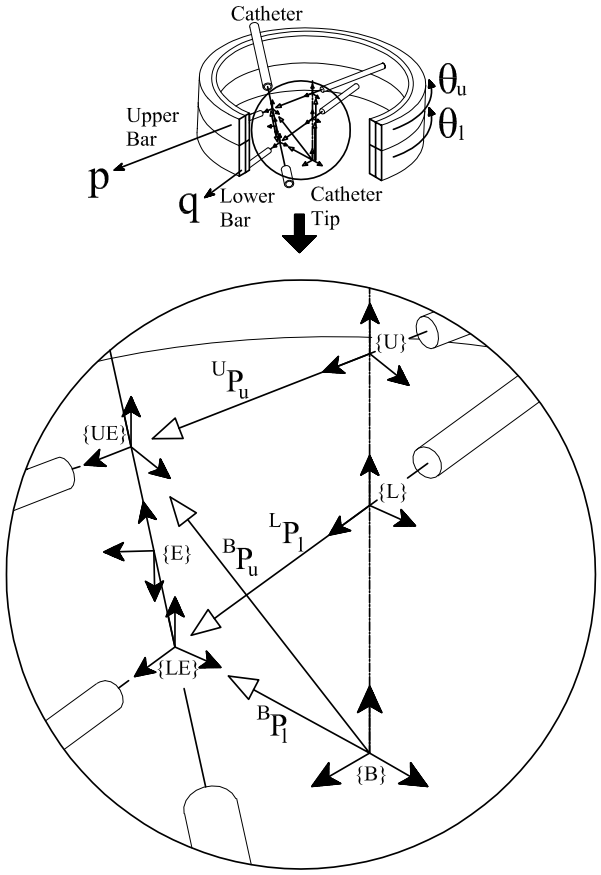

Figure 3. The coordinate system used in deriving the forward kinematics

$\{LE\}$ that have the same orientation as $\{U\}$ and $\{L\}$ do but are attached to the universal joint's center points in upper and lower levels, respectively. ${}^{B}\mathbf{P_u}$ and ${}^{B}\mathbf{P_l}$ are two vectors described in frame $\{B\}$ that point to the location of catheter holders in upper and lower levels. ${}^{U}\mathbf{P_u}$ and ${}^{L}\mathbf{P_l}$ are the same vectors described in frames $\{U\}$ and $\{L\}$, respectively. ${}^{B}\mathbf{T}_{EORG}$ is a vector that points to the catheter's center of gravity in the base frame. By manipulating these vectors and taking advantage of the relationship between them, the forward kinematics of the system can be obtained as follows

$$ {}^{B}\mathbf{P_u} = {}^{B}_{U}R\,{}^{U}\mathbf{P_u} + {}^{B}\mathbf{T}_{UORG}\,, \tag{1} $$

where ${}^{B}_{U}R$ is a mapping that represents the rotation of $\{U\}$ relative to $\{B\}$ and ${}^{B}\mathbf{T}_{UORG}$ is a vector that represents the origin of frame $\{U\}$ relative to $\{B\}$. Through several steps of mathematical manipulations, we have

$$ {}^{B}\mathbf{P_u} = \begin{bmatrix} p\cos\theta_u \\ p\sin\theta_u \\ \|{}^{B}\mathbf{T}_{UORG}\| \end{bmatrix}, \tag{2} $$

where $\|.\|$ indicates the length of a vector, θ_u represents the rotation of upper cylinder about vertical axis and p is the distance between holder and upper cylinder's center point where $\{U\}$ is attached. These joint parameters will be actively controlled at the time of manipulating the catheter. An alternative way to locate the upper tool holder is through the end-effector frame $\{E\}$ using

$$ {}^{B}\mathbf{P_u} = {}^{B}_{E}R\,{}^{E}\mathbf{P_u} + {}^{B}\mathbf{T}_{EORG}\,, \tag{3} $$

where ${}^{B}_{E}R$ represents the orientation of the catheter, ${}^{E}\mathbf{P_u}$ is the upper holder position vector in $\{E\}$ and ${}^{B}\mathbf{T}_{EORG}$ is a vector that describes the origin of frame $\{E\}$ relative to $\{B\}$. Likewise, the simplified version of this equation is

$$ {}^{B}\mathbf{P_u} = {}^{B}_{E}R\; l\;\hat{\mathbf{Z}}_{\mathbf{E}} + \begin{bmatrix} q\cos\theta_l \\ q\sin\theta_l \\ \|{}^{B}\mathbf{T}_{LORG}\| \end{bmatrix}, \tag{4} $$

where θ_l and q play the same role θ_u and p did in (2) except that they are related to lower level of the platform. In addition, in (4), l is the length of the catheter between lower and upper holders that may change with time. From (2) and (4), we have

$$ {}^{B}_{E}R\; l\;\hat{\mathbf{Z}}_{\mathbf{E}} = \begin{bmatrix} p\cos\theta_u - q\cos\theta_l \\ p\sin\theta_u - q\sin\theta_l \\ h \end{bmatrix}, \tag{5} $$

where $h = \|{}^{B}\mathbf{T}_{UORG}\| - \|{}^{B}\mathbf{T}_{LORG}\|$ is the vertical distance between upper and lower cylinders. Since any 3×3 rotation matrix can be described by only three parameters, (5) contains four unknowns including ${}^{B}_{E}R$ and l. Since the catheter does not rotate about its long axis, it only has two rotational degrees of freedom. By choosing a proper representation of its orientation, the number of unknowns in (5) can be reduced to three and hence the forward kinematic problem becomes solvable. The X-Y-Z Euler angles representation is used for this purpose [18]. Based on this representation, the final orientation of the catheter is

$$ R_{X'Y'Z'}(\alpha,\beta,0) = \begin{bmatrix} c\beta & 0 & s\beta \\ s\alpha s\beta & c\alpha & -s\alpha c\beta \\ -c\alpha s\beta & s\alpha & c\alpha c\beta \end{bmatrix}. \tag{6} $$

Finally, the series of equations to describe the forward kinematics can be expressed as follows

$$ l\sin\beta = p\cos\theta_u - q\cos\theta_l \tag{7a} $$

$$ l\sin\alpha\cos\beta = q\sin\theta_l - p\sin\theta_u \tag{7b} $$

$$ l\cos\alpha\cos\beta = h. \tag{7c} $$

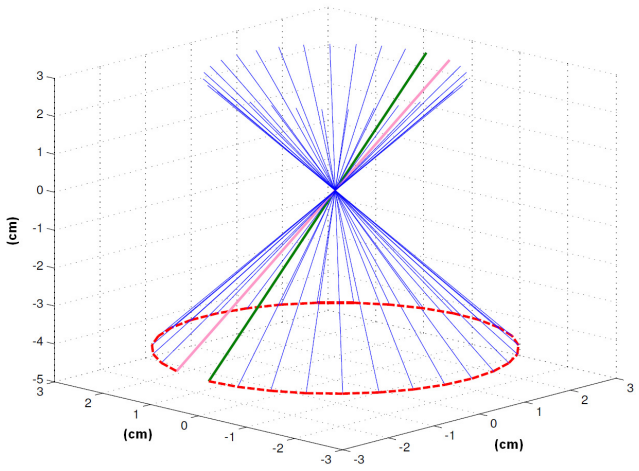

Figure 4. Simulation results to validate the forward kinematics

Solving the above equations provides the orientation parameters based on the known input distances and angles as

$$\alpha = \tan^{-1}\left(\frac{q\sin\theta_l - p\sin\theta_u}{h}\right) \tag{8a}$$

$$\beta = \tan^{-1}\left(\frac{p\cos\theta_u - q\cos\theta_l}{\sqrt{h^2 + (q\sin\theta_l - p\sin\theta_u)^2}}\right). \tag{8b}$$

In order to validate the results, a numerical model is developed in MATLAB by keeping q and θ_l to be zero while p was arbitrarily chosen to be a constant number (here 2 *cm*). Now by increasing θ_u, a full circle is swept by the tip of the catheter as expected. Figure 4 shows the position of the catheter under afore-described conditions.

Once the position of the center of mass in catheter is specified,

$${}^{B}\mathbf{T}_{EORG} = \begin{bmatrix} q\cos\theta_l - l'\sin\beta \\ q\sin\theta_l + l'\sin\alpha\cos\beta \\ \|{}^{B}\mathbf{T}_{LORG}\| - \cos\alpha\cos\beta \end{bmatrix},$$

and linear velocity and acceleration can be simply achieved through differentiating the above equation with respect to time. In this equation, l' is the constant distance between the origin of $\{LE\}$ and $\{E\}$. To obtain an expression for angular velocity and acceleration of the catheter, the relation between rotation tensor R and angular velocity is used as $\dot{R}R^{-1}\mu = \omega \times \mu$, where μ can be any arbitrary vector. Considering the fact that vector cross products can be described as the product of a skew-symmetric matrix and a vector, an explicit expression for the angular velocity of the catheter can be found as follows

$$[\omega]_\times = \begin{bmatrix} 0 & -\omega_3 & \omega_2 \\ \omega_3 & 0 & -\omega_1 \\ -\omega_2 & \omega_1 & 0 \end{bmatrix} = {}^{B}_{E}\dot{R}\ {}^{B}_{E}R^{-1}. \tag{9}$$

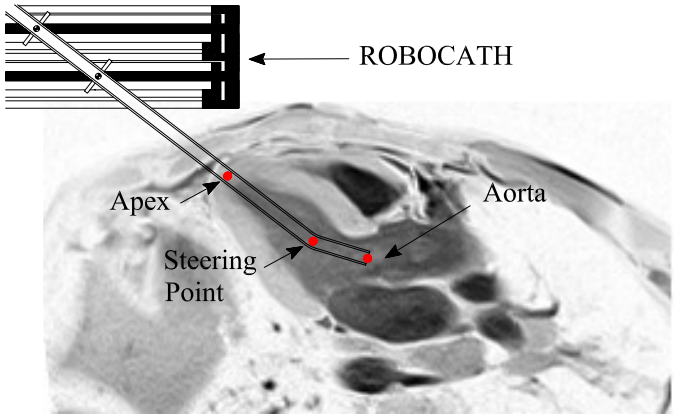

Figure 5. Set points used in reaching aortic annulus

Consequently, angular acceleration can be obtained by differentiating ω with respect to time.

3.2 Inverse kinematics

The primary objective in obtaining the inverse kinematics of any robotic platform is to connect the task space with the joint space. This enables the controller to position and orient the end effector by adjusting the joint parameters. As stated earlier, the general mission of the ROBOCATH is to drive the surgical tool to reach any arbitrary point inside the heart. However, for the particular case of aortic valve replacement operation using a transapical approach, catheter should be steered such that it could eventually reach aortic annulus. Based on the approach described in [3] and depicted in Figure 5, if the catheter passes through the apex and the steering point, it needs to be bent to access the aorta. The bending part is handled by another mechanism whose description and functionality is not within the scope of this paper. The interested reader is referred to [19] for the design and analysis of the bending part. To begin deriving the inverse kinematics equations, the frame $\{E\}$ attached to the end effector is considered based on the position of apex ${}^{B}\mathbf{P_a}$ and steering point ${}^{B}\mathbf{P_s}$ as

$$\hat{\mathbf{Z}}_E = \frac{{}^{B}\mathbf{P_a} - {}^{B}\mathbf{P_s}}{|{}^{B}\mathbf{P_a} - {}^{B}\mathbf{P_s}|} \tag{10a}$$

$$\hat{\mathbf{Y}}_E = \frac{\hat{\mathbf{X}}_B \times \hat{\mathbf{Z}}_E}{|\hat{\mathbf{X}}_B \times \hat{\mathbf{Z}}_E|} \tag{10b}$$

$$\hat{\mathbf{X}}_E = \hat{\mathbf{Y}}_E \times \hat{\mathbf{Z}}_E. \tag{10c}$$

It is worth mentioning that since the rotation matrix deduced from above unit vectors is to be compared with the Euler angle based rotation matrix obtained earlier, $\hat{\mathbf{Y}}_E$ is intentionally placed in the YZ plane in the base frame. The rotation matrix is obtained

as

$$ {}^{B}_{E}R = [\hat{\mathbf{X}}_E,\ \hat{\mathbf{Y}}_E,\ \hat{\mathbf{Z}}_E]. \tag{11} $$

Based on this description, Euler parameters α and β are

$$ \alpha = \arctan 2\left({}^{B}_{E}R(3,2), {}^{B}_{E}R(2,2)\right) \tag{12a} $$

$$ \beta = \arctan 2\left({}^{B}_{E}R(1,3), {}^{B}_{E}R(1,1)\right). \tag{12b} $$

By knowing the distal position of the end effector, as well as the parameters α and β, (7a)-(7c) can be solved to obtain joint parameters θ_l, θ_u, p and q as follows

$$ q = \mid {}^{B}\mathbf{P_a} - \frac{{}^{B}\mathbf{P_a}\cdot\hat{\mathbf{Z}}_B}{\hat{\mathbf{Z}}_E\cdot\hat{\mathbf{Z}}_B}\hat{\mathbf{Z}}_E \mid \tag{13a} $$

$$ \theta_l = \arccos\left(\frac{\left({}^{B}\mathbf{P_a} - \frac{{}^{B}\mathbf{P_a}\cdot\hat{\mathbf{Z}}_B}{\hat{\mathbf{Z}}_E\cdot\hat{\mathbf{Z}}_B}\hat{\mathbf{Z}}_E\right)\cdot\hat{\mathbf{X}}_B}{\mid {}^{B}\mathbf{P_a} - \frac{{}^{B}\mathbf{P_a}\cdot\hat{\mathbf{Z}}_B}{\hat{\mathbf{Z}}_E\cdot\hat{\mathbf{Z}}_B}\hat{\mathbf{Z}}_E \mid}\right) \tag{13b} $$

$$ \theta_u = \arctan\left(\frac{q\sin\theta_l - h\tan\alpha}{h\frac{\tan\beta}{\cos\alpha} + q\cos\theta_l}\right) \tag{13c} $$

$$ p = \frac{q\sin\theta_l - h\tan\alpha}{\sin\theta_u}. \tag{13d} $$

It should be noted that there are some singularity issues in solving the inverse kinematic of the robot such as when the catheter passes through origin of lower and upper frames; however, such issues are numerically treatable. In addition, the general issue of having more than one solution to the inverse problem can be addressed by restricting the end effector to pass through two set points rather than one.

4 Driving and Control of ROBOCATH Prototype

The prototyped model of ROBOCATH shown in Figure 6 weighs less than 300 g that makes it appropriate to serve as a patient-mounted platform. This version of the robot is fully made of Acrylonitrile Butadiene Styrene (ABS plastic) and manufactured through rapid prototyping with the exception of the guide bars that have a significant impact on robot performance and are chosen from a special type of polyamides known as Torlon. This self-lubricating plastic shows reasonably high stiffness and tensile strength and hence is suitable for our application. Geometric parameters of the model are provided in Table 3.

The currently utilized driving and control system depicted in Figure 7 consists of a power supply, motor driver boards, data acquisition system, control boards, stepper motors and transmission system. Stepper motors are utilized in this study simply because of their ease of use compared to DC motors. In spite of the fact that the robot requires four motors to be fully actuated, in this study, we use only two motors to make the actuation less

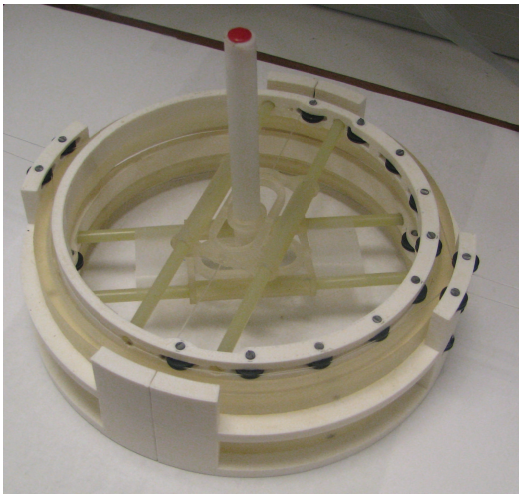

Figure 6. Prototyped model of the platform

Table 3. Prototype specifications

Feature	Size (mm)
Outer diameter of the casing	165
Inner diameter of the rotating ring	120
Height of the platform	45.5
Diameter of the catheter	10

complicated. To this end, two DOFs need to be fixed including the robots' lower level rotational and translational degrees of freedom. The idea of placing the actuators far from the scanner area enables us to employ conventional electric motors to drive the robot. However, this arrangement necessitates the development of a cable transmission configuration that allows one to remotely control the platform. Currently utilized transmission system employs two closed chains of plastic ropes for each level of the platform. In Figure 8, which schematically shows the transmission system for one of the levels, the closed chains numbered 1 and 2 correspond to linear and rotational degrees of freedom, respectively. These chains transmit the power from stepper motors (numbered 5 and 6) to the corresponding connection points on the mechanism (numbered 3 and 4). Different sets of pulleys that are considered in between, not only guide the cables to pass the desired paths (7 and 8), but also significantly reduce the friction (9). While this configuration successfully satisfies the actuation requirements, the coupling between rotational and linear DOFs should be effectively addressed in the controller design process to achieve the desired performance.

In the literature, several control strategies have been proposed to satisfy requirements of parallel platforms [20]. In this paper, we employ a simple ON/OFF feedback control along with a feedforward to compensate for the coupling between linear and

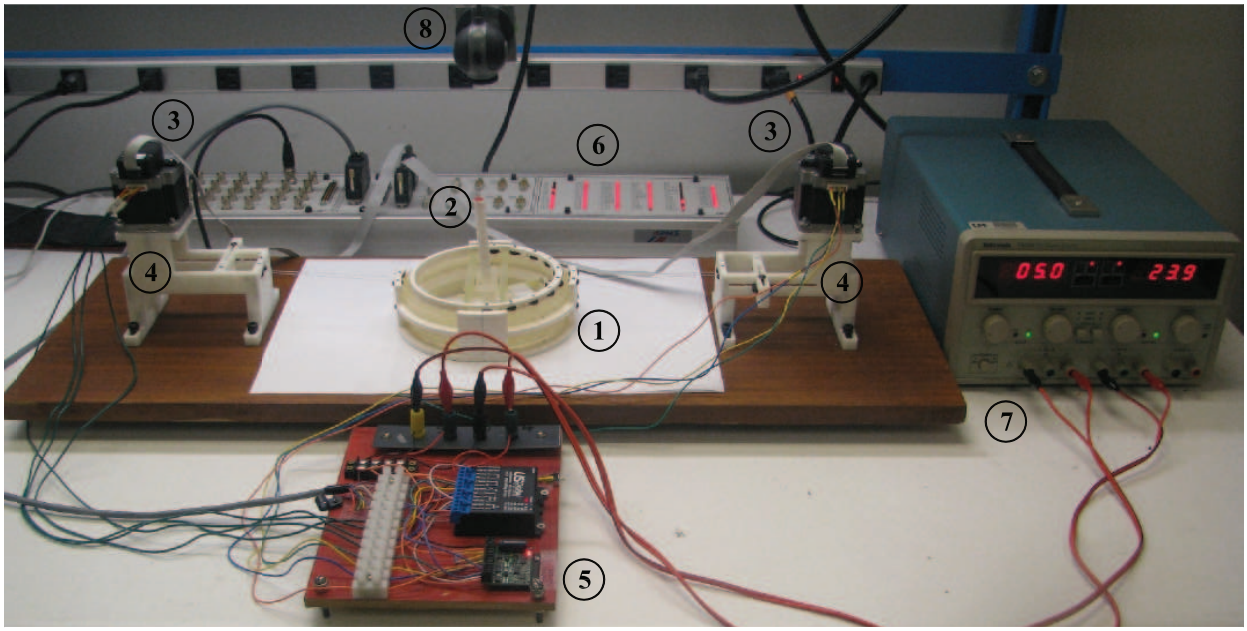

Figure 7. Experimental setup including: (1) platform, (2) marker, (3) stepper motors, (4) transmission system, (5) motor driver board, (6) dSPACE real-time control and data acquisition system, (7) power supply, (8) camera

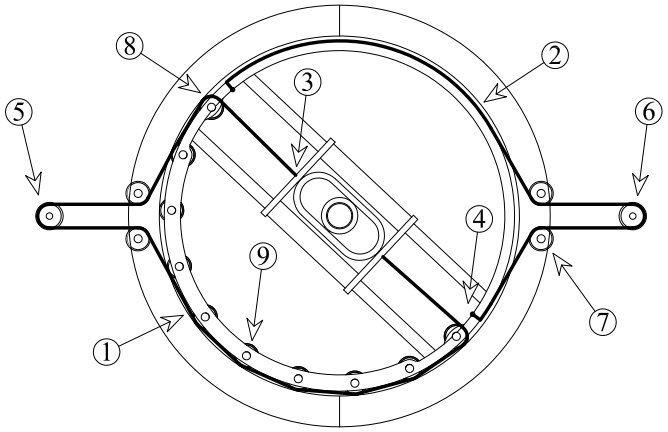

Figure 8. Transmission system

Figure 9. Image processing in MATLAB

rotational DOFs. Actuation command signals are generated initially in MATLAB and then transmitted to motor drivers through dSPACE acting as our real-time control and data acquisition system. Imaging section of the experimental setup consists of a camera placed above the robot to capture the position of the marker (as shown in Figure 9). Based on the experiment, this marker could be attached either to the distal part of the catheter or to the upper holder. Using MATLAB image processing toolbox, the position of the center point of this marker is tracked. In order to achieve on-the-fly control of the platform, imaging should be executed in real-time. However, in current setup, due to the lack of precision of the used camera, feedback signals are provided by the stepper motors' built-in encoders. Imaging, on the other hand, is done off-line to capture the motion of the platform. The path lines originated by these images will serve as experimental results in the next section. In the ideal case, we will: (i) use DC motors instead of stepper motors, (ii) actuate all the four available DOFs, and (iii) use the MR image data instead of the encoders' data.

5 Evaluation of the Design Performance

To evaluate the performance of the developed system, three different sets of experiments are defined and the corresponding results are discussed in this section. The experiments are de-

signed to address some of the important issues such as coupling between degrees of freedom, accuracy and repeatability in tracking set points and reference trajectories.

5.1 Compensation of the DOFs coupling using feedforward controls

Combination of rotational and translational degrees of freedom at each level of the platform enables the robot to position the catheter holders in desired polar coordinates. The undesired coupling of the degrees of freedom should be taken care of to prevent distorted motion of the platform. To properly address DOF coupling issue in this experiment, the platform is commanded to move the catheter such that its upper holder moves on a quarter of a circle's perimeter positioned at the center of the rotating ring (from point 1 to point 2 in Figure 10). To capture the motion of the holder, the imaging maker is attached to it. Failing to resolve the coupling issue leads to the deviation of the holder from the desired path (dashed line in Figure 10), where it passes through the origin (point **c**) and stops at the other side of the cylinder plane (point 2'). Adding a feedforward control action compensates for the interference by transmitting proper actuation signals to the stepper motor corresponding to the translational DOF. The perfect arc-shaped motion of the holder after applying this corrective feedforward control (solid line in Figure 10) results in a significant improvement in the navigation of the robot and ensures the effectiveness of the proposed compensation scheme.

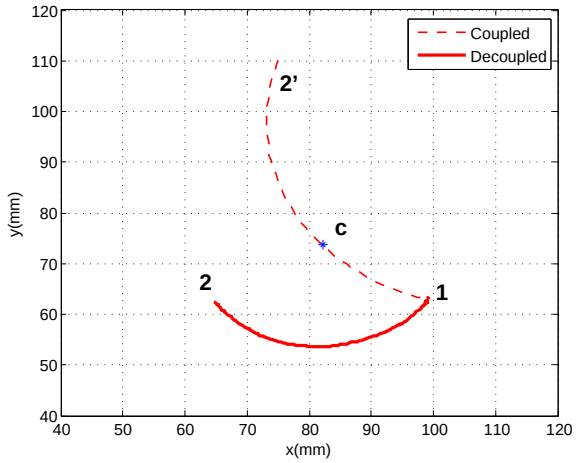

Figure 10. DOF coupling cancellation

5.2 Reference set point tracking

Within the feedback control law, a threshold level is defined to adjust the accuracy of the system in following the set points. Once the error between the encoder measurements and the reference data exceeds this amount, the actuation signal will be cut off. In the case of utilizing stepper motors, this actuation signal is the pulse frequency that magnetizes the stepper motors' coils and dictate the angular velocity. In this experiment, a four-node closed contour is defined by its corners' polar coordinates. Feeding the controller with this data, this test is performed to examine the accuracy of the robot in following such reference inputs. To capture the motion of the end effector, the marker is placed on the distal end of the catheter. While all the set points are reached by the robot as illustrated in Figure 11, the irregular motion of the holder between the set points that does not follow any patterns makes this method less appealing for the trajectory tracking purpose. Another interesting observation is the marker's profile between upper and lower set points. This is due to discontinuity in rotational degree of freedom that only covers the interval $(0, \pi)$ and prevents the platform to connect upper and lower points with a straight line or an arc. In fact, in order to connect any points in the upper sector of the plane to the lower part, all trajectories have to pass through the center point of the ring. Due to the specific application of the ROBOCATH, in which the catheter is aimed to follow off-center miniature contours, this issue does not affect the performance of the platform.

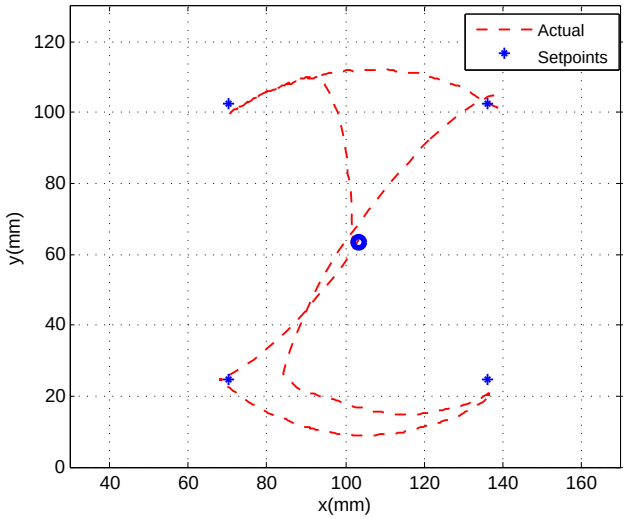

Figure 11. Set point tracking

5.3 Reference trajectory tracking

Continuous trajectory tracking leads to higher computational costs and hence requires more elaborate control efforts compared to the set points tracking. However, the manipulability is significantly extended by this method and the irregular motions of the end effector will no longer appear in the results. To evaluate the accuracy of the platform in following the reference trajectories and also to assess the effectiveness of the implemented control scheme, an arbitrarily chosen zigzag path is considered as the input signal. Utilizing the inverse kinematic model of the platform developed earlier, the controller commands the joint

such that the desired path is swept by the end effector. Figure 12 shows both the reference path and the platform output, which is the contour that the marker has passed. The maximum error is observed to be less than 1 mm. While this error is partially due to the control deficiencies, as well as the mechanical issues such as backlash, the contribution of other hardware including camera should also be taken into account. In fact, by filtering the perspective effect in the captured images, the obtained results will be significantly improved.

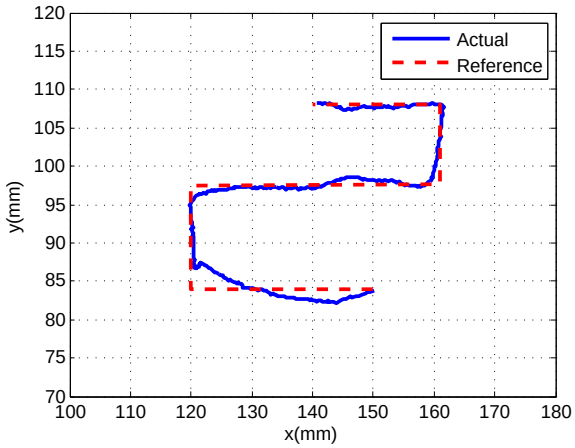

Figure 12. Trajectory tracking

The final experiment introduced in this study is used to examine the repeatability. For this purpose, a circular trajectory in the upper level of the platform is swept by the holder in three consecutive intervals. The captured contours are depicted in Figure 13. The maximum deviation that any of these three paths have produced relative to the others does not exceed 2 mm, while the maximum deviation from the reference input is observed to be 3 mm. This interesting observation, once again, highlights the major contribution of the imaging issue in generating the errors. In addition, the sufficiently close compliance of swept trajectories guarantees the high level of repeatability in the system. The encoder measurements corresponding to this trajectory are shown in Figure 14. While the motor actuating the linear DOF closely follows the reference signal, the other actuator partially fails to track the input, especially around the peak points. This is due to the speed limitations of the stepper motors. We expect that implementing an advanced control method by utilizing DC motors will lead to resolving this problem.

6 Conclusion and Future Work

Beating heart interventions using a transapical approach offer several advantages including less patient's recovery time compared to the traditional procedures. However, issues such as the moving boundaries of the work space need to be carefully addressed to achieve the desired outcomes. In this paper,

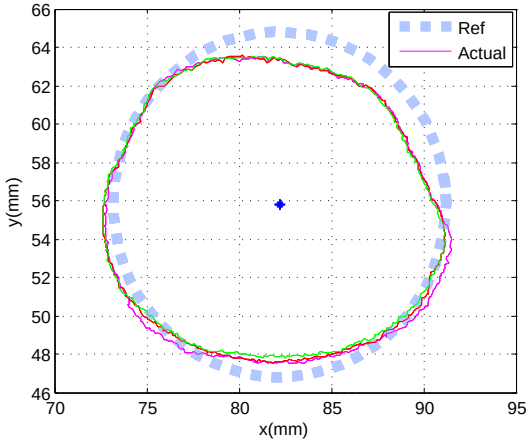

Figure 13. Repeatability test

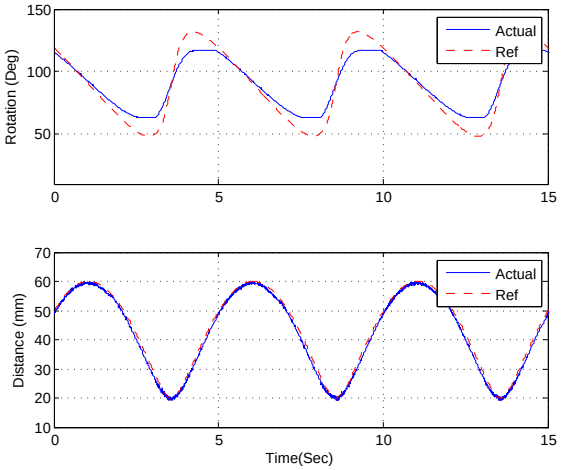

Figure 14. Encoder measurements

we propose the design of a robotic platform that could fit the requirements of such sophisticated and minimally-invasive interventions. Being equipped with MRI as the image modality, ROBOCATH is capable of positioning and orienting the cardiac catheter to avoid any collision between the interventional tool and the internal organs under beating heart condition. Operational needs such as MRI-compatibility, chest's relative motion compensation, accuracy and compactness are also properly taken care of in design of the platform. Development of the platform's kinematic model further enables us to ensure that kinematic requirements are met prior to manufacturing the robot. The inverse model is later employed by the controller to allow for reference trajectory tracking. To validate the ROBOCATH design concept and test the prototype model, an experimental setup is developed. Three sets of experiments are designed to evaluate the system performance by implementing a feedback control combined with a corrective feedforward term to compensate for the DOFs coupling issue. These experiments collectively illustrate

the effectiveness of the controller in canceling the coupling, the acceptable accuracy and repeatability of the platform in tracking the reference set points and trajectories.

The authors are currently conducting additional experiments to utilize advanced model-based controls for disturbance attenuation and tracking the reference trajectories generated from the MRI images taken and processed on-the-fly. In addition, to make the mechanism ready to assist with aortic valve replacement procedure, additional degrees of freedom corresponding to the insertion of the catheter and its navigation inside left ventricle are being added to the top of current platform.

Acknowledgment

This work was supported by the National Science Foundation under Grant CNS-0932272. All opinions, findings, conclusions or recommendations expressed in this work are those of the authors and do not necessarily reflect the views of the sponsor. The authors would like to thank Prof. Heidar Malki at the UH department of engineering technology for providing access to the machine shop.

REFERENCES

[1] Nof, S., 1999. *Handbook of industrial robotics*, Vol. 1. John Wiley & Sons.

[2] Hockstein, N., Gourin, C., Faust, R., and Terris, D., 2007. "A history of robots: from science fiction to surgical robotics". *Journal of robotic surgery,* **1**(2), pp. 113–118.

[3] Yeniaras, E., Lamaury, J., Deng, Z., and Tsekos, N., 2010. "Towards a new cyber-physical system for MRI-guided and robot-assisted cardiac procedures". In Proc. IEEE International Conf. on Information Technology and Applications in Biomedicine.

[4] Tsekos, N., Khanicheh, A., Christoforou, E., and Mavroidis, C., 2007. "Magnetic resonance-compatible robotic and mechatronics systems for image-guided interventions and rehabilitation: a review study". *Annu. Rev. Biomed. Eng.,* **9**, pp. 351–387.

[5] Atluri, P., Kozin, E., Hiesinger, W., and Joseph Woo, Y., 2009. "Off-pump, minimally invasive and robotic coronary revascularization yield improved outcomes over traditional on-pump cabg". *International Journal of Medical Robotics and Computer Assisted Surgery,* **5**(1), pp. 1–12.

[6] Li, M., Mazilu, D., and Horvath, K., 2008. "Robotic system for transapical aortic valve replacement with MRI guidance". *Medical Image Computing and Computer-Assisted Intervention–MICCAI 2008*, pp. 476–484.

[7] Li, M., Kapoor, A., Mazilu, D., and Horvath, K., 2011. "Pneumatic actuated robotic assistant system for aortic valve replacement under MRI guidance". *Biomedical Engineering, IEEE Transactions on,* **58**(2), pp. 443–451.

[8] Yeniaras, E., Lamaury, J., Navkar, N., Shah, D., Chin, K., Deng, Z., and Tsekos, N., 2011. "Magnetic resonance based control of a robotic manipulator for interventions in the beating heart". In Robotics and Automation (ICRA), 2011 IEEE International Conference on, IEEE, pp. 6270–6275.

[9] Susil, R., Krieger, A., Derbyshire, J., Tanacs, A., Whitcomb, L., Fichtinger, G., and Atalar, E., 2003. "System for MR image–guided prostate interventions: Canine study". *Radiology,* **228**(3), p. 886.

[10] Kim, D., Kobayashi, E., Dohi, T., and Sakuma, I., 2002. "A new, compact MR-compatible surgical manipulator for minimally invasive liver surgery". *Proc. Medical Image Computing and Computer-Assisted Intervention (MICCAI)*, pp. 99–106.

[11] Muntener, M., Patriciu, A., Petrisor, D., Mazilu, D., Bagga, H., Kavoussi, L., Cleary, K., and Stoianovici, D., 2006. "Magnetic resonance imaging compatible robotic system for fully automated brachytherapy seed placement". *Urology,* **68**(6), pp. 1313–1317.

[12] Stoianovici, D., Song, D., Petrisor, D., Ursu, D., Mazilu, D., Mutener, M., Schar, M., and Patriciu, A., 2007. "MRI stealth robot for prostate interventions". *Minimally Invasive Therapy & Applied Technologies,* **16**(4), pp. 241–248.

[13] Berkelman, P., Cinquin, P., Troccaz, J., Ayoubi, J., Letoublon, C., and Bouchard, F., 2002. "A compact, compliant laparoscopic endoscope manipulator". In Proc. IEEE Int. Conf. on Robotics and Automation (ICRA), Vol. 2, pp. 1870–1875.

[14] Berkelman, P., Troccaz, J., and Cinquin, P., 2004. "Body-supported medical robots: A survey". *Journal of Robotics and Mechatronics,* **16**(5), pp. 513–519.

[15] Maurin, B., Bayle, B., Piccin, O., Gangloff, J., de Mathelin, M., Doignon, C., Zanne, P., and Gangi, A., 2008. "A patient-mounted robotic platform for CT-scan guided procedures". *IEEE Trans. Biomedical Engineering,* **55**(10), pp. 2417–2425.

[16] Schauer, D., Hein, A., and Lueth, T., 2003. "Robopoint–an autoclavable interactive miniature robot for surgery and interventional radiology". In International Congress Series, Vol. 1256, Elsevier, pp. 555–560.

[17] Schauer, D., Hein, A., and Lüth, T., 2003. "Dynamic force control for a miniaturised medical robot system". In Advanced Intelligent Mechatronics, 2003. AIM 2003. Proceedings. 2003 IEEE/ASME International Conference on, Vol. 2, IEEE, pp. 1090–1095.

[18] Craig, J., 2004. "Introduction to robotics: mechanics and control".

[19] Salimi, A., Mohammadpour, J., Grigoriadis, K., and Tsekos, N., 2011. "Dynamic simulation of blood flow effects on flexible manipulators during intra-cardiac procedures on the beating heart". In Proc. ASME. Dynamic Systems and Control Conference, Arlington, VA.

[20] Merlet, J., 2006. *Parallel robots*. Springer-Verlag New York Inc.